Preliminary experience of cardiac proton spectroscopy at 0.75 T

Journal Article

Author(s):
Peereboom, Sophie M.; Guenthner, Christian; Albannay, Mohammed; Kozerke, Sebastian

Publication date:
2023-07

Permanent link:
https://doi.org/10.3929/ethz-b-000594616

Originally published in:
NMR in Biomedicine 36(7), https://doi.org/10.1002/nbm.4892

Received: 30 March 2022 | Revised: 10 November 2022 | Accepted: 9 December 2022

DOI: 10.1002/nbm.4892

RESEARCH ARTICLE

NMR IN BIOMEDICINE WILEY

Preliminary experience of cardiac proton spectroscopy at 0.75 T

Sophie M. Peereboom | Christian Guenthner | Mohammed M. Albannay | Sebastian Kozerke

Institute for Biomedical Engineering, University and ETH Zurich, Zurich, Switzerland

Correspondence
Sebastian Kozerke, Institute for Biomedical Engineering, University and ETH Zurich, Gloriastrasse 35, 8092 Zurich, Switzerland.
Email: kozerke@biomed.ee.ethz.ch

Recent work on high-performance lower-field MR systems has renewed the interest in assessing relative advantages and disadvantages of magnetic fields less than 1 T. The objective of the present work was to investigate signal-to-noise ratio (SNR) scaling of point-resolved spectroscopy as a function of field strength and to test the feasibility of proton MRS of triglycerides (TGs) in human in vivo myocardium at 0.75 T relative to 1.5 T and 3 T. Measurements at 0.75 T were obtained by temporarily ramping down a clinical 3 T MR scanner. System configurations at 0.75, 1.5 and 3 T featured identical hard- and software, except for differences in transmit/receive coil geometries and receive channel count, which were accounted for in SNR comparisons. Proton MRS was performed at 0.75 T, 1.5 T and 3 T in ex vivo tissue and in vivo calf muscle to measure T_1 and T_2 values as a function of field strength, which in turn served as input to simulations of SNR scaling and field-dependent TG fit errors. Preliminary in vivo spectra of myocardium were acquired at 0.75 T, 1.5 T and 3 T in healthy subjects. Measurements of both ex vivo tissue and in vivo muscle tissue at 0.75 T versus 1.5 T and 3 T confirmed decreasing T_1 and increasing T_2^* for decreasing field strengths. Using measured T_1, T_2 and T_2^* as input and using field-dependent echo time and bandwidth scaling, simulated Cramér-Rao lower bounds of TG amplitudes at 0.75 T were 2.3 and 4.5 times larger with respect to 1.5 T and 3 T, respectively. In vivo measurements demonstrate that human proton spectroscopy of TGs in cardiac muscle is feasible at 0.75 T, supporting the potential practical value of lower-field high-performance MR systems.

KEYWORDS
cardiac muscle, heart, lower-field MR, PRESS, proton spectroscopy, triglyceride

Abbreviations: [1]H-MRS, proton MRS; CR, creatine; CRLB, Cramér-Rao lower bound; ECG, electrocardiogram; EMCL, extramyocellular lipid; IMCL, intramyocellular lipid; NSA, number of signal averages; PRESS, point-resolved spectroscopy; SAR, specific absorption rate; SNR, signal-to-noise ratio; T_E, echo time; TG, triglyceride; TMA, trimethylammonium; T_R, repetition time.

1 | INTRODUCTION

Proton (^{1}H) MRS has shown promise to assess cardiac metabolism of healthy and diseased hearts.[1] The main metabolites of interest are total creatine (CR) and triglycerides (TGs), which are found to be altered in cases of heart failure, infarction and different types of cardiomyopathy.[2–4] Increased levels of TG correlate to impaired myocardial function in patients with diabetes mellitus or metabolic syndrome,[5–7] underlining the importance of intramyocardial lipid quantification.

Today's clinical MR is primarily performed at 1.5 T or 3 T, and, lately, also at 7 T. Higher field strengths come with the advantage of higher thermal polarization and therefore higher signal-to-noise ratios (SNRs) along with larger peak separation in spectroscopy. These benefits are, however, partly counterbalanced by larger field inhomogeneities, higher specific absorption rates (SARs) and consequently longer RF pulse durations. Additionally, potential electrocardiogram (ECG) mis-triggering due to an increased magnetohydrodynamic effect[8] can compromise the robustness of cardiac MRS at high fields.

In contrast, lower field strengths can benefit from lower SAR levels. To this end, the RF duration can be shortened, which in turn allows reduction of echo times, and, in conjunction with steady/increased T_2 values[9,10] at lower fields, leads to SNR gains relative to classical field-strength dependent SNR scaling.[11] Depending on the repetition time, the decrease in T_1 values at lower static fields can be SNR advantageous as well. The reduced spectral separation at lower field can be partly compensated by smaller linewidths due to more homogeneous intravoxel phasing and therefore higher T_2^* values. In addition, chemical shift artefacts decrease with lower magnetic field strengths for a given RF pulse bandwidth, leading to improved spatial localization. From the perspective of patient comfort, acoustic noise is reduced at lower fields due to reduced Lorentz forces on the gradient coils.[12,13] From an economical point of view, lower-field MRI systems come with an intrinsically lower cost, opening up possibilities for improved accessibility to MRI scanners.

Despite the promises of lower fields, commercial low-field systems are traditionally equipped with lower-performance RF amplifiers, gradient drivers and receiver hardware. However, recent work on ramped-down high-performance MRI systems has renewed the interest in reassessing advantages and disadvantages of lower-field MRI. Cardiac cine imaging and assessment of cardiac function, blood flow and myocardial tissue relaxation parameters have been performed on commercial 0.35 T systems[14,15] and on custom-designed 0.55 T instrumentation.[16,17] Lower-field MRI has been pointed out to offer advantages for MR-guided cardiovascular interventions, imaging of high-susceptibility regions and sampling-efficient acquisition methods. However, the feasibility of in vivo human cardiac ^{1}H spectroscopy at lower fields has not yet been demonstrated.

Accordingly, the objective of the present study was to investigate the feasibility of ^{1}H-MRS for the assessment of TGs of cardiac muscle on a custom 0.75 T MRI system in comparison with measurements on clinical 1.5 T and 3 T systems with identical hard- and software. Simulations based on measured T_1, T_2 and T_2^* values were performed to assess SNR dependences on field strength, and ^{1}H spectra acquired in human myocardium at 0.75 T versus 1.5 T and 3 T are presented.

2 | METHODS

2.1 | Experimental setup

A 3 T Achieva scanner (Philips Healthcare, Best, the Netherlands) was ramped down to a field strength of 0.75 T. The target field strength of 0.75 T, i.e., a quarter of 3 T, allowed the use of the scanner's ^{13}C multi-nuclei hardware for transmit and receive ($\gamma_{13C} \approx \frac{1}{4}\gamma_{1H}$) on protons. For transmit, a custom-built double Helmholtz pair-like two-loop coil (Clinical MR Solutions, Brookfield, WI, USA) was employed, while a four-channel

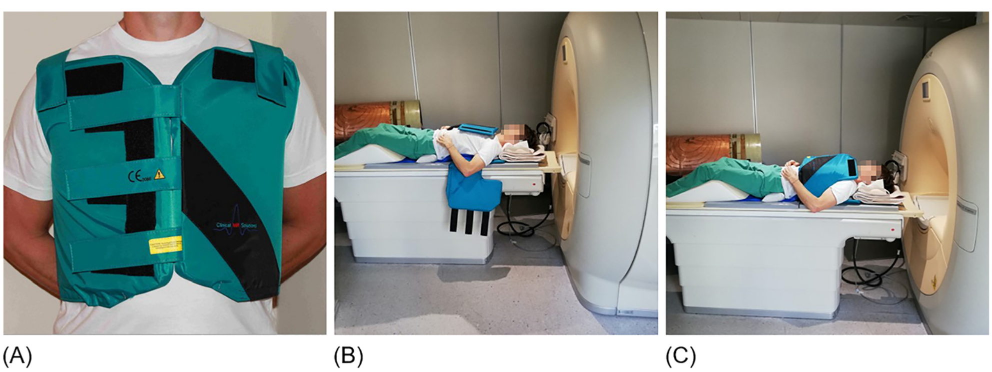

FIGURE 1 Experimental setup: a custom-made double Helmholtz transmitter and a four-channel receive coil array, originally designed to measure ^{13}C at 3 T, were used to acquire ^{1}H images and spectra at 0.75 T.

local receive array (Clinical MR Solutions) with two posterior and two anterior elements was used for signal reception at 0.75 T (Figure 1). Shim iron placement on the shim rails was re-optimized for the lowered field strength, compensating for both static field inhomogeneity and fields induced by the fixed 3 T factory shims that are bolted to the cryostat. The 3 T ^{1}H body coil could not be used and remained disconnected inside the scanner during the 0.75 T experiments. Changes in pulse sequence programming encompassed (1) adjustment of γ to calculate correct fields, (2) overwriting resonance frequency ranges to allow values outside the normal 3 T ranges and (3) adaptation of preparation phases for automatic frequency, transmit power, shim and receive gain adjustment using the local coils instead of the body coil.

Comparative measurements were performed on both a 1.5 T Philips Achieva scanner using a five-channel cardiac receiver array and a 3 T Philips Achieva scanner using a two-channel receiver coil (phantom and calf muscle measurements) and a six-channel cardiac receiver array (cardiac measurements). All scanner configurations featured identical software versions and gradient settings (gradient strength of 31 mT/m at a slew rate of 200 T/m/s).

2.2 | Ex vivo measurements

Phantom measurements were performed at room temperature in duck breast. Prior to all spectroscopic measurements, first-order pencil-beam volume shimming was carried out.[18,19] Spectra were acquired using a point-resolved spectroscopy (PRESS) sequence[20] in a voxel volume of $10 \times 20 \times 40$ mm^3. The bandwidth BW was set to 1000, 2000 and 4000 Hz at 0.75 T, 1.5 T and 3 T, respectively, and $N_s = 512$ samples were acquired. The repetition time T_R was 2000 ms. A schematic diagram of the pulse sequence at the different field strengths including scaling of B_1^+ is shown in Figure 2. Peak B_1 ($B_{1\,max}$) was scaled inversely with B_0 according to

$$B_{1max} = \frac{40.5\,\mu\mathrm{T}}{B_0}. \tag{1}$$

Accordingly, minimum echo times T_E were 15, 18 and 26 ms at 0.75, 1.5 and 3 T, respectively.

Series with different echo times (T_E range = 15–26, …, 400 ms, 11 steps) and repetition times (T_R range = 375–5000 ms, nine steps) were acquired without water suppression (number of signal averages (NSA) = 8) to determine the T_1 and T_2 of tissue water at 0.75, 1.5 and 3 T. Water-suppressed spectra were acquired using chemical-shift selective water suppression[21] (excitation bandwidth of 200 Hz at 3 T, 100 Hz at 1.5 T and 50 Hz at 0.75 T) with NSA set to 48. To determine T_2 of TG the series with different echo times was repeated with water suppression.

2.3 | Numerical simulations

To assess field-dependent SNR scaling and TG fit errors, simulation code was implemented in MATLAB (MathWorks, Natick, MA, USA). Six intramyocardial resonances were simulated (residual water at 4.7 ppm, TGs at 2.1, 1.3 and 0.9 ppm, CR at 3.0 ppm and trimethylammonium

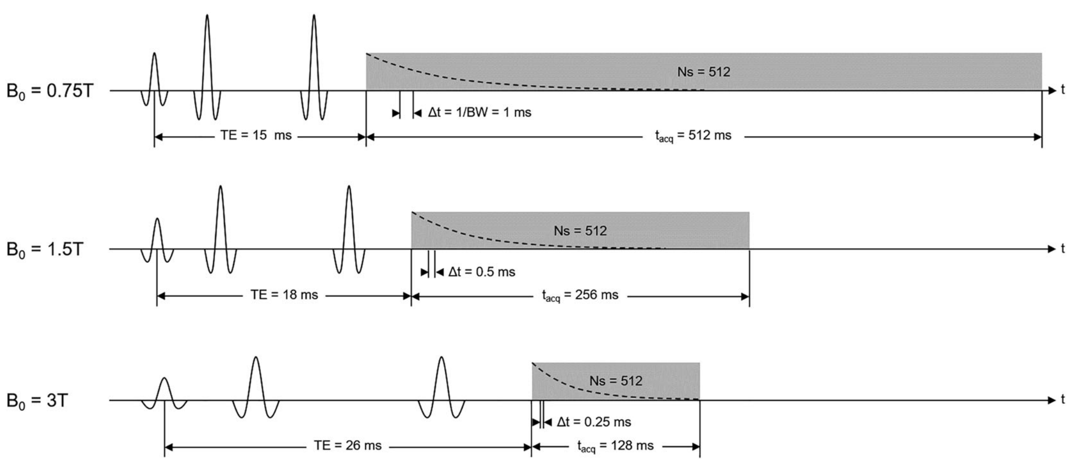

FIGURE 2 Schematic diagram of echo time- and bandwidth-adapted PRESS pulse sequence for different field strengths. The peak radiofrequency amplitude B_1^+ is scaled inversely with B_0, resulting in reduced echo times T_E with decreasing field strengths. The bandwidth BW$= 1/t_{acq}$ is proportionally reduced as B_0 decreases, while the number of sampling points (N_s) is kept constant.

(TMA) at 3.2 ppm) assuming PRESS volume selection and FID acquisition with $N_s = 512$ samples. Signals and noise were calculated for 0.75 T, 1.5 T and 3 T based on Equations (A1)–(A9) as found in the appendix for two different scenarios: (a) $T_E \propto B_0$,$\mathrm{BW} \propto B_0$ and (b) $T_E = T_{E,3T} = \mathrm{const}$, $\mathrm{BW} = \mathrm{BW}_{3T} = \mathrm{const}$, the latter assuming no field-dependent change of T_E and BW. Relaxation parameter scaling of tissue water and TG was derived from the duck breast data and all sequence parameters were set according to values as used in the ex vivo measurements. T_1 of TG was assumed to be sufficiently short for all field strengths to allow complete relaxation between acquisitions.[22,23]

The time-domain SNR (SNR_{TD})[24] was calculated as the absolute signal of the first point of the FID divided by the standard deviation of the noise. Amplitudes and T_2* were fitted in the time domain using a gradient-free simplex search method and fit errors are reported relative to ground truth. Cramér-Rao lower bounds (CRLBs) of the TG resonances were derived using the Hessian of the fit cost function. Simulations were repeated 500 times for statistics.

Relative differences in time-domain SNR_{TD} with $T_E \propto B_0$, $BW \propto B_0$ were compared with experimental data of water signals acquired without water suppression in the ex vivo duck breast at 0.75 T, 1.5 T and 3 T as outlined in the previous section. To account for differences in the receive coils used at the different field strengths, the coil geometries were modeled in CST Microwave Studio (Dassault Systèmes, Vélizy-Villacoublay, France). The coil elements were excited with a broadband current source to ensure uniform current density along the element conductors. Coil elements were individually phased accordingly to resemble the excitation profile observed from experimental data. The simulated coil sensitivity maps can be found in the Supporting Information.

2.4 | In vivo measurements

Measurements were made in both calf muscle and the interventricular septum of three healthy volunteers upon written informed consent and according to ethics and institutional guidelines. All spectra were acquired with a voxel size of $10 \times 20 \times 40\ \mathrm{mm}^3$ (8 mL), bandwidths of 1000, 2000 and 4000 Hz at 0.75 T, 1.5 T and 3 T, respectively, and 512 samples, i.e. settings identical to the ex vivo measurements. First-order pencil-beam volume shimming was performed using a $15 \times 25 \times 45\ \mathrm{mm}^3$ shim volume. Local power optimization was achieved by monitoring the intensity of the water peak for a series of incrementing flip angles of both excitation and refocusing pulses.[25] Measurements in the same subject across field strengths were performed within the time frame of one week.

For the calf measurements, the MRS voxel was positioned in the soleus muscle (see Figure 5A later) and data were acquired with a T_R of 2000 ms. For cardiac measurements, the MRS voxel was positioned in the interventricular septum (see Figure 8A later) using short-axis and long-axis cine balanced steady-state free precession images acquired in a breath hold. Cardiac PRESS data acquisition was ECG-triggered to end systole with a minimum T_R of 2000 ms. Water suppression in the heart was performed with a modified excitation bandwidth of 100 Hz at 0.75 T and a frequency offset of 25 Hz, given that the smaller water suppression pulse bandwidths did not fit the time available between the R-peak and end systole. Respiratory gating was performed using a navigator positioned on the right (1.5 T, 3 T) or left (0.75 T) hemidiaphragm (gating window = 4 mm).[26] A total of 192 water-suppressed and 16 water-unsuppressed averages were acquired. All other parameters were identical to those used in the ex vivo measurements. Finally, image-based T_1 mapping (modified Look–Locker inversion recovery (MOLLI), $T_R = 3.0$ ms, flip angle = 25°, reconstructed voxel size = $1.4 \times 1.4 \times 20\ \mathrm{mm}^3$) was performed in one midventricular slice in a breath hold.

2.5 | Reconstruction

All spectra were reconstructed in MATLAB with a reconstruction pipeline developed and implemented in ReconFrame (GyroTools LLC, Winterthur, Switzerland). Noise decorrelation was performed; water-unsuppressed averages were used to calculate coil channel weights and coil combination was achieved using a singular value decomposition approach.[27] Water-unsuppressed averages were phased on the individual water peaks before averaging; water-suppressed averages were phased on the main TG resonance at 1.3 ppm.[28] Individual water-unsuppressed averages were frequency corrected based on the water signal and the average water frequency shift was used to correct all water-suppressed averages. Eddy current correction was performed by subtracting the phase of the average water signal from both the water-suppressed and water-unsuppressed signals.[29]

2.6 | Data analysis

Water spectra were fitted with Lorentzian line shapes in the time-domain using AMARES[30] (jMRUI,[31] Version 5.2) and linewidth was assessed. Water amplitudes acquired with different repetition times were fitted according to the following function:

$$M_z(TR, T_1) = a\left(1 - b\left(e^{-\frac{TR}{T_1}}\right)\right) \tag{2}$$

with a, b and T_1 being fit parameters. T_2 was acquired by fitting the data from the T_E series:

$$M_{xy}(T_E, T_2) = a\left(e^{-\frac{T_E}{T_2}}\right) \tag{3}$$

and T_2^* was calculated based on the linewidth LW of the water peaks according to

$$\mathrm{LW} = \frac{1}{\pi T_2^*}. \tag{4}$$

T_1, T_2 and T_2^* were fitted as functions of magnetic field according to $T_1 = a(B_0)^b$, $T_2 = c(B_0)^d$ and $T_2^* = e(B_0)^f$, respectively. Residual water peaks were removed from the duck breast, calf and heart metabolite spectra using Hankel Lanczos singular value decomposition (HLSVD) in AMARES. Cardiac spectra were fitted using five resonances: TGs at 0.9, 1.3 and 2.1 ppm, CR at 3.0 ppm and TMA at 3.2 ppm. Spectra acquired in the calf muscle were fitted with resonances at 0.9 ppm (intramyocellular lipid (IMCL) –CH_3), 1.3 ppm (IMCL–CH_2), 1.1 ppm (extramyocellular lipid (EMCL) –CH_3), ~1.5 ppm (EMCL–CH_2), 3.0 ppm (CR–CH_3), 3.2 ppm (TMA) and 2.1 ppm (TGs). CR–CH_3 and TMA were fitted using Lorentzian line shapes, whereas all lipid peaks were fitted with Gaussian shapes. Relative chemical shifts were fixed except for EMCL, as the chemical shift of EMCL–CH_2 can vary as a function of the angle between the muscle and B_0.[32] Relative phases were set to zero for all metabolites; there were no restrictions for linewidths and amplitudes.

Additionally, TGs (defined as the sum of the fitted resonances at 0.9 and 1.3 ppm) in spectra acquired in the duck breast with different echo times were fitted according to Equation (3). ΔB_0 was calculated for the different field strengths based on T_2 and T_2* values of the water signal, enabling estimation of T_2* values of TG.

A region of interest was drawn in the septal region of the T_1 maps to derive myocardial T_1. All variables are presented as mean ± standard deviation.

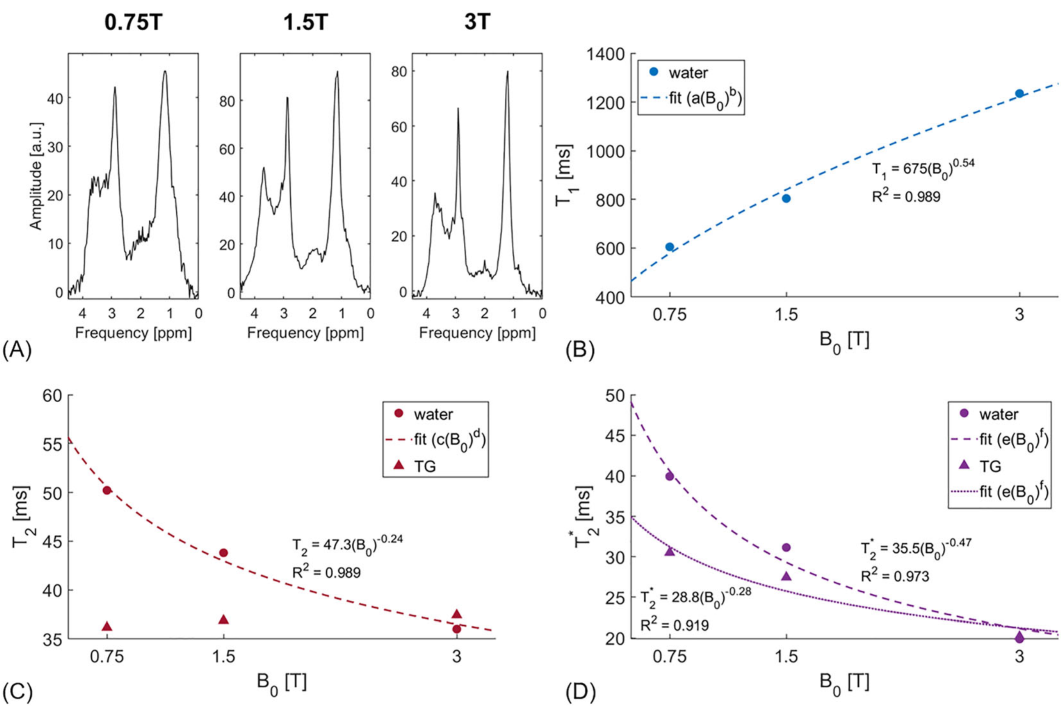

FIGURE 3 (A) Spectra acquired in an ex vivo duck breast at 0.75 T, 1.5 T and 3 T. B–D, T_1 (B), T_2 (C) and T_2* (D) dependences on field strength for water and main TG signals. R^2 values are given for all fits.

3 | RESULTS

Figure 3 shows the T_1, T_2 and T_2^* values of the ex vivo duck breast fitted as a function of magnetic field. Data were fitted as $T_1 = 675(B_0)^{0.54}$ ($R^2 = 0.989$, water), $T_2 = 47.3(B_0)^{-0.24}$ ($R^2 = 0.989$, water), $T_2^* = 35.5(B_0)^{-0.47}$ ($R^2 = 0.973$, water) and $T_2^* = 28.8(B_0)^{-0.28}$ ($R^2 = 0.919$, TG). T_2 of TG was approximately constant for all field strengths. Measured T_1, T_2 and T_2* values of the water and main TG signals are given in Table 1.

Figure 4 shows simulated SNR_{TD} as a function of magnetic field as calculated according to Equations (A1)–(A9) and T_1, T_2 and T_2^* values as presented in Figure 3. It can be seen that scaling of both T_E and BW with B_0 reduces SNR_{TD} losses at lower field when compared with the case where both T_E and BW are constant for all field strengths (Figure 4A and 4D). Using field-dependent echo time and bandwidth scaling, simulated SNR_{TD} at 0.75 T is 75.4% of SNR at 1.5 T and 68.5% of SNR at 3 T. This as opposed to using constant T_E and BW, where SNR_{TD} at 0.75 T is 48.6% and 25.5% of SNR at 1.5 T and 3 T, respectively. Fit errors of TG amplitude and T_2^* are shown in Figure 4B and 4C. Reduction of T_E and BW for decreased field strengths reduces fit errors and relative CRLBs (Figure 4B, 4C, 4E and 4F). Scaling of both T_E and BW with B_0 leads to simulated CRLBs of TG amplitudes that are 2.3 and 4.5 times larger at 0.75 T with respect to 1.5 T and 3 T, respectively, and simulated CRLBs of T_2^*

TABLE 1 Measured T_1, T_2 and T_2* values of the water and main TG signals of an ex vivo duck breast at 0.75 T, 1.5 T and 3 T.

	0.75 T	1.5 T	3 T
T_1 (water) [ms]	604.7	803.6	1234.0
T_2 (water) [ms]	50.2	43.8	36.0
T_2 (TG) [ms]	36.2	36.9	37.4
T_2* (water) [ms]	39.9	31.2	19.9
T_2* (TG) [ms]	30.5	27.5	20.2

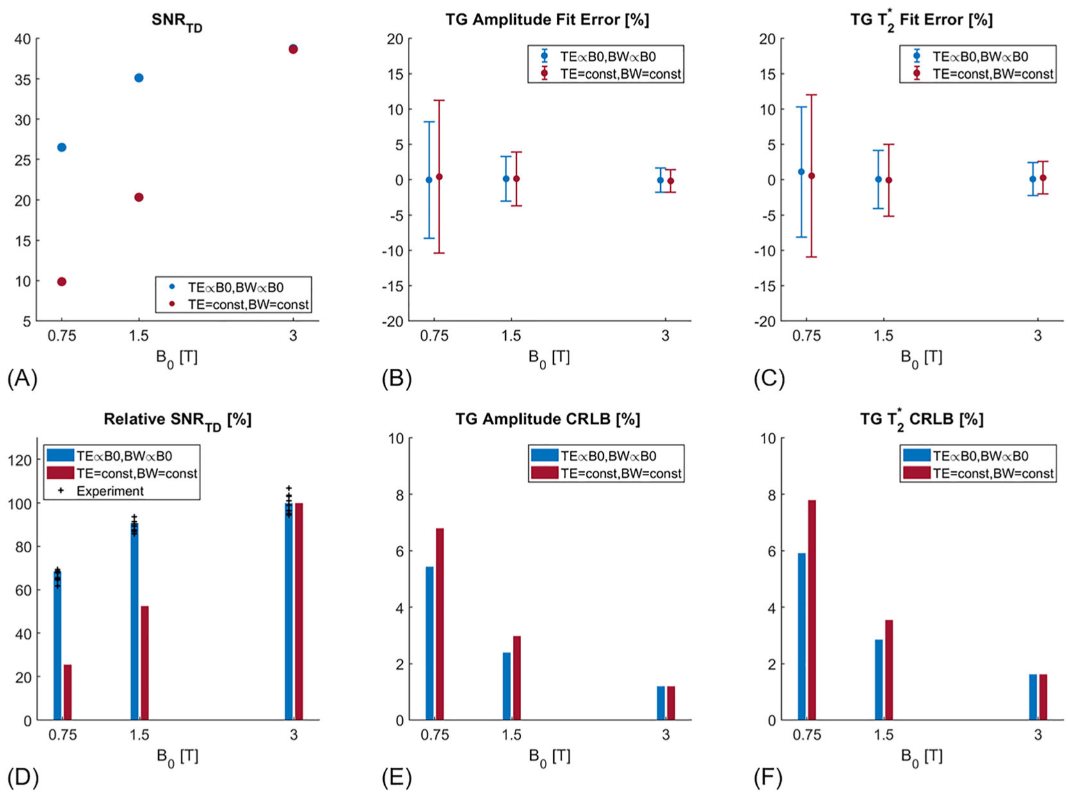

FIGURE 4 (A) Simulated SNR_{TD} for 0.75 T, 1.5 T and 3 T based on field-dependent relaxation parameters determined in ex vivo experiments comparing echo time and bandwidth adapted (blue) versus PRESS with echo time and bandwidth values fixed to 3 T (red). (B, C) Fitting errors of TG resonance amplitudes and T_2*. (D–F) Relative SNR_{TD} (D) representing the integral over all resonances and CRLBs of TG amplitudes and T_2* (E, F); black crosses in D represent experimental data of eight averages of water signals derived from ex vivo duck measurements without water suppression and normalized to the mean of SNR_{TD} obtained at 3 T.

that are 2.1 and 3.6 times larger at 0.75 T compared with 1.5 T and 3 T, respectively. Experimental data of relative SNR_{TD} derived from ex vivo duck breast measurements are provided in Figure 4D for comparison (black crosses).

Exemplary spectra acquired from the soleus muscle at 0.75 T, 1.5 T and 3 T are shown in Figure 5B; Figure 5C and 5D shows the fitted components, the estimated spectra and the residuals of the fits. CR can be distinguished at all field strengths. The lipid–CH_2 peak cannot be separated into IMCL and EMCL with the current protocols and experimental setup.

In Figure 6 T_1, T_2 and T_2^* dependences on field strength for the water signal of in vivo calf muscle are presented. The relationship between relaxation parameters and field strength is given by $T_1 = 887(B_0)^{0.35}$ ($R^2 = 0.989$), $T_2 = 36.5(B_0)^{-0.21}$ ($R^2 = 0.979$) and $T_2^* = 30.2(B_0)^{-0.12}$

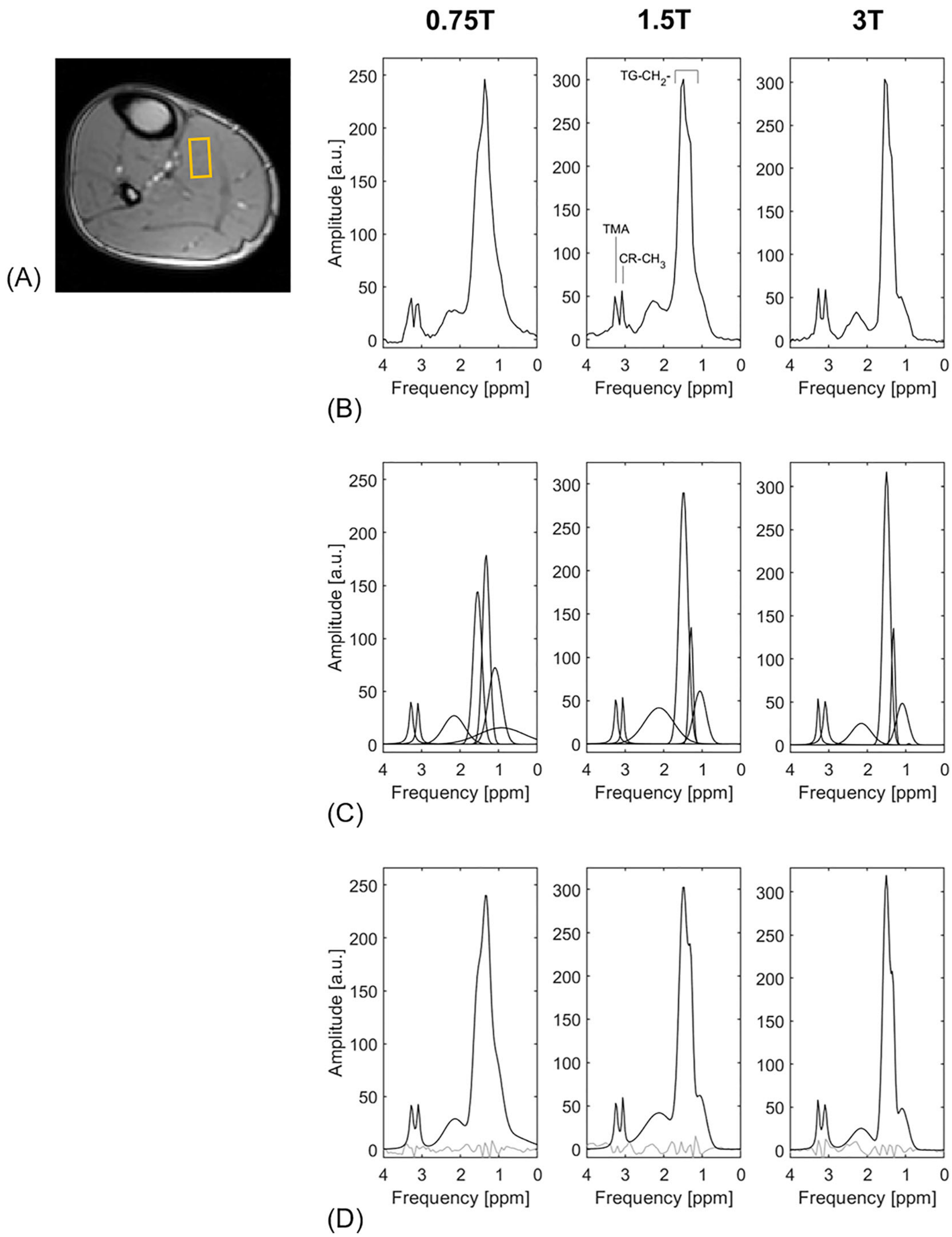

FIGURE 5 (A) Positioning of a 10 × 20 × 40 mm^3 voxel in the soleus muscle. The image was acquired at a field strength of 1.5 T. (B) Exemplary spectra acquired in the calf muscle of the same subject at 0.75 T, 1.5 T and 3 T. (C, D) Fitted components (C) and estimated spectra (D) together with residuals of the fits. CR can be distinguished. The lipid CH_2–peak cannot be separated into IMCL and EMCL.

($R^2 = 0.854$). This corresponds to water peak linewidths of 10.37 ± 0.29 Hz at 0.75 T, 10.65 ± 0.29 Hz at 1.5 T and 12.23 ± 0.43 Hz at 3 T. Measured T_1, T_2 and T_2* values of the water signal are given in Table 2.

Exemplary cardiac short-axis and four-chamber cine images of one volunteer acquired at 0.75 T, 1.5 T and 3 T are shown in Figure 7. High intensities close to the flexible transmit/receive coils were observed at 0.75 T, while more homogeneous excitation was obtained at 1.5 T and 3 T given the presence of a body coil. Image quality was sufficient at all field strengths to ensure adequate planning of the MRS voxel.

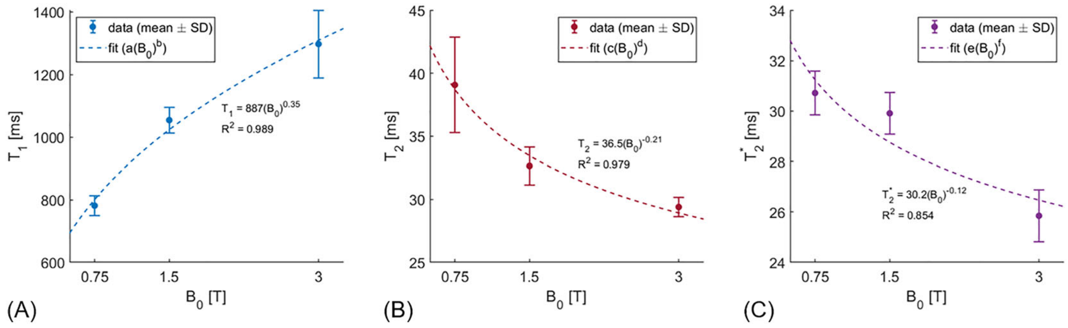

FIGURE 6 T_1 (A), T_2 (B) and T_2* (C) dependences on field strength of the water signal of in vivo soleus muscle. Data are shown as mean ± standard deviation over all volunteers ($n = 3$). R^2 values are given for all fits.

TABLE 2 Measured T_1, T_2 and T_2* values of the water signal of in vivo soleus muscle at 0.75 T, 1.5 T and 3 T. Values are shown as mean ± standard deviation over all volunteers ($n = 3$).

	0.75 T	1.5 T	3 T
T_1 (water) [ms]	781.4 ± 31.3	1054.3 ± 41.1	1297 ± 108.4
T_2 (water) [ms]	39.1 ± 3.8	32.7 ± 1.5	29.6 ± 1.1
T_2* (water) [ms]	30.7 ± 0.9	29.91 ± 0.8	25.9 ± 1.0

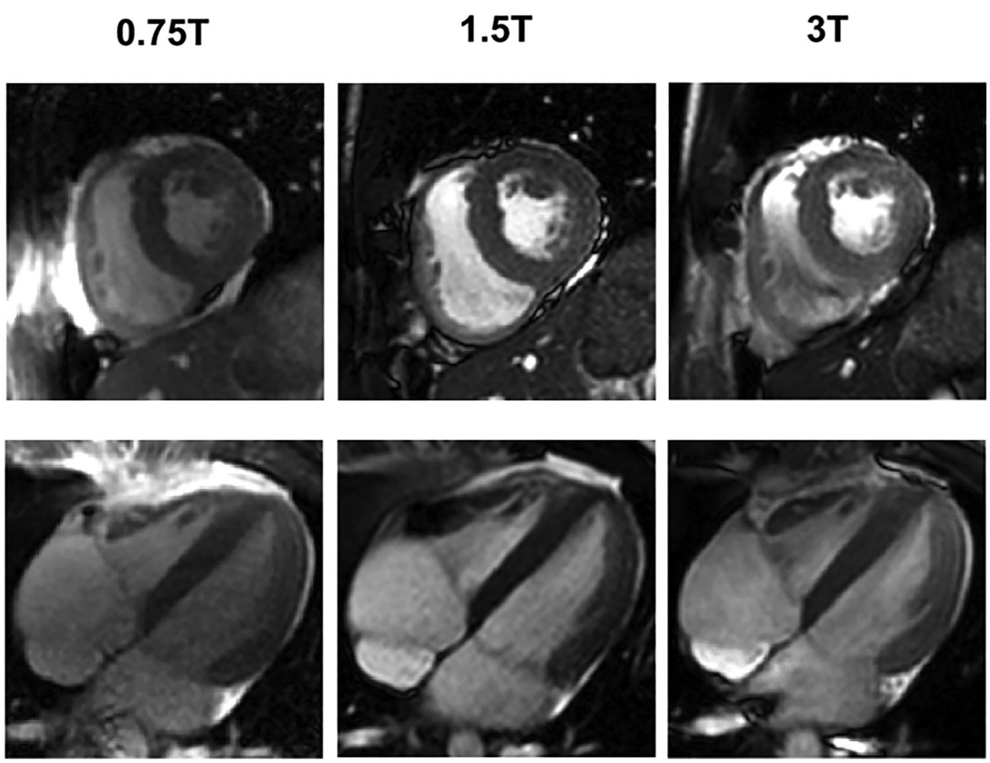

FIGURE 7 Exemplary cardiac short-axis and four-chamber cine images of one subject acquired at 0.75 T, 1.5 T and 3 T as used to plan the MRS voxel. Signal intensity is less homogeneous for 0.75 T as compared with 1.5 T and 3 T, given the lack of a body coil and therefore less homogeneous RF transmission.

Figure 8B compares exemplary spectra acquired in the interventricular septum at different field strengths. Figure 8C and 8D shows the fitted components, the estimated spectra and the residuals of the fits. Despite the decrease in peak separation at lower field strengths, relevant metabolites can be detected in the heart at 0.75 T.

T_1 maps acquired in one volunteer at different field strengths are shown in Figure 9A. T_1 shows a dependence on B_0 according to $T_1 = 864(B_0)^{0.27}$ with $R^2 = 0.947$ (Figure 9B). Figure 9C shows T_2* of myocardial water fitted as a function of magnetic field strength ($T_2^* = 45.2(B_0)^{-0.50}$, $R^2 = 0.995$). This corresponds to linewidths of 6.22 ± 0.74 Hz (0.75 T), 8.40 ± 0.51 Hz (1.5 T) and 12.65 ± 1.57 Hz (3 T). Measured T_1 and T_2* values of the water signal are given in Table 3.

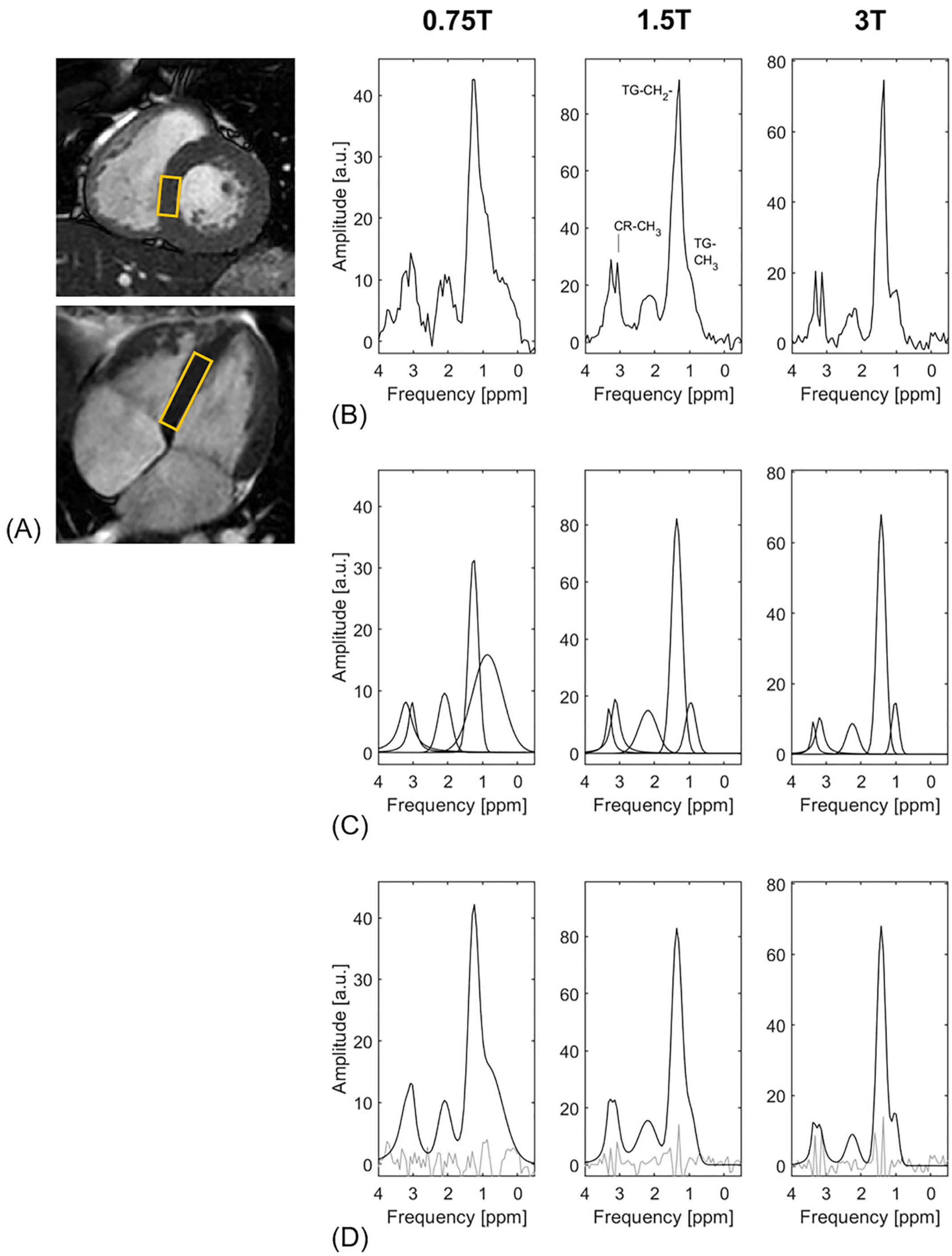

FIGURE 8 (A) Positioning of a 10 × 20 × 40 mm^3 voxel in the interventricular septal wall. The images were acquired at a field strength of 1.5 T. (B) Exemplary cardiac spectra of one subject acquired at 0.75 T, 1.5 T and 3 T. (C, D) Fitted components (C) and estimated spectra together with residuals of the fits (D).

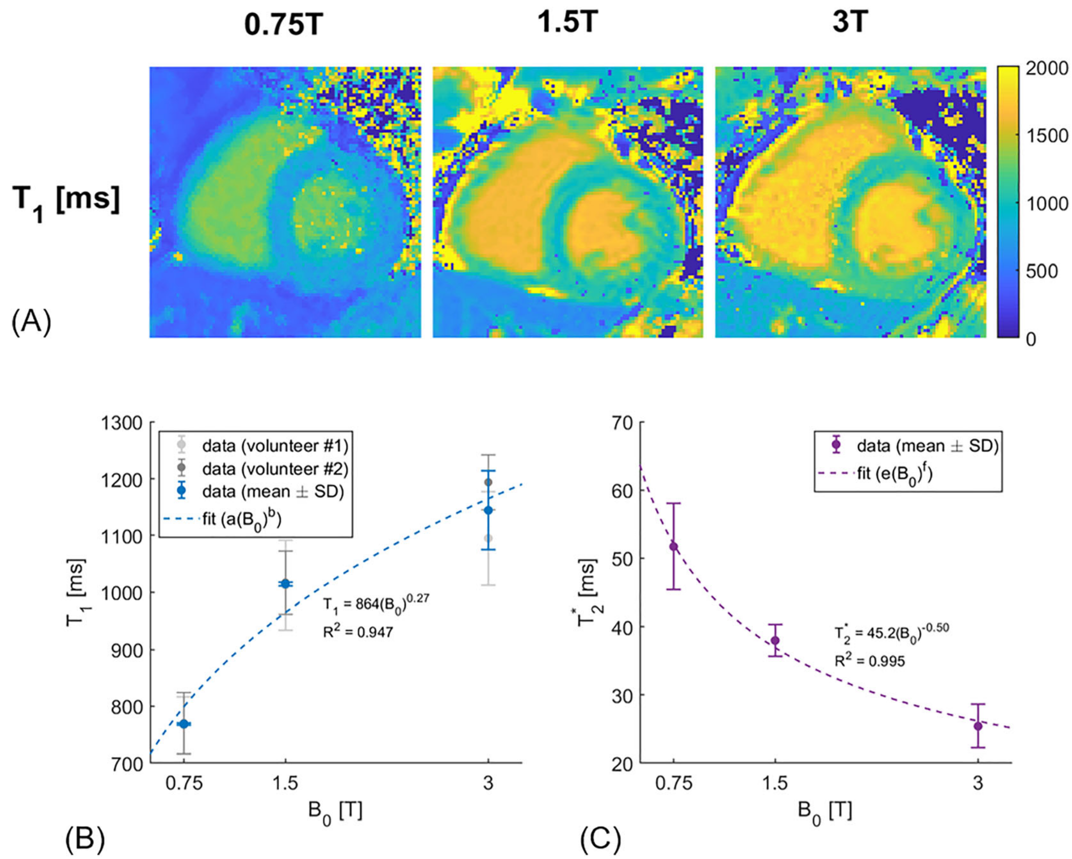

FIGURE 9 (A) T_1 maps acquired in the heart at different field strengths. (B) T_1 dependence on field strength for a region in the myocardial septum. Data from two volunteers are shown in grey as mean ± standard deviation over all voxels in the selected regions. (C) T_2* dependence on field strength of the water signal of the interventricular septum. Data are shown as mean ± standard deviation over all volunteers; R^2 values of the fits are given.

TABLE 3 Measured T_1 and T_2* values of the water signal of the interventricular septum at 0.75 T, 1.5 T and 3 T. Values are shown as mean ± standard deviation over all volunteers.

	0.75 T	1.5 T	3 T
T_1 (water) [ms]	768.9 ± 2.3	1015 ± 3.5	1144 ± 69.7
T_2* (water) [ms]	51.7 ± 6.3	38.0 ± 2.3	25.4 ± 3.2

4 | DISCUSSION

In this work we report our preliminary experience with cardiac ^{1}H spectroscopy on a clinical 3 T MR system ramped down to 0.75 T relative to measurements at 1.5 T and 3 T. Data on the field dependence of T_1, T_2 and T_2* values were obtained and used as input to simulations to provide insights into SNR scaling and TG fit errors of point-resolved MRS as a function of static field strengths. To assess data quality as a function of field strength, CRLBs of data fitting were calculated to avoid dependences on whether signal and noise are measured in the time domain or frequency domain.[24]

While the field-dependent T_1 of the water signal of the ex vivo duck breast scaled approximately with the square root of B_0 (Figure 3B), both in vivo calf muscle (Figure 6A) and myocardium (Figure 9B) showed a stronger field dependence of T_1 on B_0, in agreement with findings from literature.[22] Since a T_R of 2000 ms was used in our simulations and measurements, the increased T_1 at higher field contributed to the non-linear scaling of the time-domain SNR as a function of field strength (Figure 4A and 4D).

Water signal T_2 of the ex vivo duck breast and in vivo calf muscle increased with decreasing field with approximately the fourth to fifth root (Figures 3C and 6B), while TG T_2 was largely independent of B_0 (Figure 3C), a finding that agrees with data from literature where TGs in human skeletal muscle were investigated.[23] To this end, the scaling of time-domain SNR (Figure 4A and 4D), when adapting T_E and bandwidth relative to fixed T_E and bandwidth, is explained. At the same time, the comparatively smaller reduction in TG fit error when adapting T_E and bandwidth is related to the almost constant T_2 of TG as a function of field strength and the fact that the time-domain SNR represents the integral signal of all resonances present in the spectrum.

Relative differences in time-domain SNR_{TD} with $T_E \propto B_0, BW \propto B_0$ were compared with experimental data of water signals acquired without water suppression in the ex vivo duck breast at 0.75 T, 1.5 T and 3 T.

An SNR comparison was made between simulations and experimental water-unsuppressed data acquired in the ex vivo duck breast for the case where $T_E \propto B_0, BW \propto B_0$. Corrections for the different numbers of coil elements and geometries as used at the three different field strengths were applied, assuming voxel placement exactly in the center of the coil elements. SNR comparisons were not made for in vivo measurements; confounders such as motion artifacts and differences in coil positioning between field strengths would have compromised a fair SNR comparison.

Although peak separation in units of hertz reduces linearly with decreasing field strength, longer T_2* made spectral quality adequate to distinguish relevant metabolites in our work. However, scaling of T_2* varied considerably. While T_2* of tissue water increased with decreasing field with approximately the square root in the ex vivo duck breast (Figure 3D) and in vivo myocardium (Figure 9C), only weak scaling was found in the in vivo calf muscle experiment (Figure 6C), a finding that we associate in part with inconsistent shimming across the in vivo calf muscle experiments.

Besides challenges with the automatic shimming procedure at 0.75 T given the surface transmit/receive coil configuration, the limited transmit field homogeneity and power available at 0.75 T also posed a challenge to B_1 power calibration. Together with the relatively small receiver elements and therefore reduced sensitivity for regions outside the heart, it resulted in difficulties in acquiring a reliable navigator signal for respiratory triggering/gating on the right hemidiaphragm. Therefore the navigator had to be positioned on the left hemidiaphragm, which made respiratory gating possible for measurements at 0.75 T. Navigator-free metabolite-cycled cardiac spectroscopy as described by Peereboom et al.[33] was not performed in the present study since the transition bandwidth of the inversion pulse needed for metabolite cycling was not sufficiently narrow to ensure correct cycling of TG at 0.75 T.

Water suppression can be challenging at lower field strengths, as spectral separation is reduced. However, the narrower peaks as a result of longer T_2* values are at the same time advantageous for water suppression. In this study, a detailed assessment of water suppression in vivo was unfortunately not possible due to experimental constraints. Based on the observed relative ratios of CR and TMA peak amplitudes relative to TG, it is believed that erroneous suppression of metabolites was not critical. This aspect needs to be studied in more detail in a future study.

Based on the time-averaged RF power equation (Equation A10), RF pulse lengths depend on the square of ω and hence B_0. However, on the scanner a linear relationship between pulse length and B_0 was implemented. This was due to the maximum RF amplifier power limit of 4 kW on the 0.75 T system.

To avoid contamination of spectra of calf muscle, care was taken not to include fasciae when positioning the MRS voxel.[34] As these fasciae were hardly visible in the MR images used for planning, some contamination of the spectra cannot be excluded. The choice of the soleus muscle for the measurements in the calf muscle was, together with a relatively large voxel, not optimal to draw conclusions on IMCL and EMCL separation. As the fibers of the soleus muscle are anatomically almost at the magic angle relative to the direction of the B_0 field, the separation of IMCL and EMCL is minimal, and they cannot be distinguished reliably. A future study should be conducted using smaller voxels in the tibialis anterior muscle, where the separation of IMCL and EMCL peaks is more pronounced.

In the heart, intra- and extra-cellular lipids are difficult to distinguish since there is no common fiber orientation. The asymmetrical lipid peaks seen in the cardiac spectra can at this moment not be explained and further research is necessary to assess this observation.

It has been shown that cardiac TG levels are dependent on circadian rhythm.[35] The study setup did not allow the same subject to be scanned on the same day and at the same time of the day at all three scanners, which might have led to TG/W variations between different field strengths.

Both calf muscle and cardiac spectra were fitted with only relative chemical shifts and line shapes as prior knowledge; linewidths and amplitudes were unconstrained. More robust fits, as would be required for studies involving a larger number of subjects, require a larger amount of prior knowledge. The amount of data presented here is, however, not sufficient to determine a correct set of constraints for the different field strengths, and the spectra with according fits should be seen as an example of feasibility.

The number of volunteers measured in this study was relatively small and did not allow for reproducibility and statistical analyses. This limitation was governed by the short trial duration in which the clinical 3 T system was ramped down to 0.75 T before being brought back to the original field strength. More volunteers would also be needed to examine whether CR can be reliably distinguished from TMA at 0.75 T.

5 | CONCLUSION

The SNR loss predicted for lower field strengths based on classical field-strength dependent SNR scaling can be partly counteracted by considering favorable relaxation properties and by exploiting shorter RF pulses, making human in vivo cardiac ^{1}H spectroscopy feasible at 0.75 T.

ORCID

Sophie M. Peereboom https://orcid.org/0000-0002-7786-3088
Christian Guenthner https://orcid.org/0000-0001-8707-7016

REFERENCES

1. van Ewijk PA, Schrauwen-Hinderling VB, Bekkers SCAM, Glatz JFC, Wildberger JE, Kooi ME. MRS: a noninvasive window into cardiac metabolism. *NMR Biomed*. 2015;28(7):747-766. doi:10.1002/nbm.3320
2. Neubauer S. The failing heart—an engine out of fuel. *N Engl J Med*. 2007;356(11):1140-1151. doi:10.1056/NEJMra063052
3. Bottomley PA, Weiss RG. Non-invasive magnetic-resonance detection of creatine depletion in non-viable infarcted myocardium. *Lancet*. 1998; 351(9104):714-718. doi:10.1016/S0140-6736(97)06402-7
4. Nakae I, Mitsunami K, Yoshino T, et al. Clinical features of myocardial triglyceride in different types of cardiomyopathy assessed by proton magnetic resonance spectroscopy: comparison with myocardial creatine. *J Card Fail*. 2010;16(10):812-822. doi:10.1016/j.cardfail.2010.05.006
5. Bizino MB, Hammer S, Lamb HJ. Metabolic imaging of the human heart: clinical application of magnetic resonance spectroscopy. *Heart*. 2014;100(11): 881-890. doi:10.1136/heartjnl-2012-302546
6. Lingvay I, Raskin P, Szczepaniak LS. The fatty hearts of patients with diabetes. *Nat Rev Cardiol*. 2009;6(4):268-269. doi:10.1038/nrcardio.2009.30
7. Nyman K, Granér M, Pentikäinen MO, et al. Cardiac steatosis and left ventricular function in men with metabolic syndrome. *J Cardiovasc Magn Reson*. 2013;15(1):103. doi:10.1186/1532-429X-15-103
8. Niendorf T, Winter L, Frauenrath T. Electrocardiogram in an MRI environment: clinical needs, practical considerations, safety implications, technical solutions and future directions. In: *Advances in Electrocardiograms—Methods and Analysis*. InTech; 2012:309-324.
9. Pohmann R, Speck O, Scheffler K. Signal-to-noise ratio and MR tissue parameters in human brain imaging at 3, 7, and 9.4 Tesla using current receive coil arrays. *Magn Reson Med*. 2016;75(2):801-809. doi:10.1002/mrm.25677
10. Krššák M, Lindeboom L, Schrauwen-Hinderling V, et al. Proton magnetic resonance spectroscopy in skeletal muscle: experts' consensus recommendations. *NMR Biomed*. 2020;34(5):e4266. doi:10.1002/nbm.4266
11. Hoult DI, Richards RE. The signal-to-noise ratio of the nuclear magnetic resonance experiment. *J Magn Reson*. 1976;24:71-85.
12. Marques JP, Simonis FFJ, Webb AG. Low-field MRI: an MR physics perspective. *J Magn Reson Imaging*. 2019;49(6):1528-1542. doi:10.1002/jmri.26637
13. Dillinger H, Kozerke S, Guenthner C. Direct comparison of gradient modulation transfer functions and acoustic noise spectra of the same MRI at high-(3T) and lower-field (0.75T). In: *Proceedings of the 29th Annual Meeting of ISMRM*. 2021:3089.
14. Simonetti OP, Ahmad R. Low-field cardiac magnetic resonance imaging: a compelling case for cardiac magnetic resonance's future. *Circ Cardiovasc Imaging*. 2017;10(6):e005446. doi:10.1161/CIRCIMAGING.117.005446
15. Varghese J, Craft J, Crabtree CD, et al. Assessment of cardiac function, blood flow and myocardial tissue relaxation parameters at 0.35 T. *NMR Biomed*. 2020;33(7):e4317. doi:10.1002/nbm.4317
16. Bandettini WP, Shanbhag SM, Mancini C, et al. A comparison of cine CMR imaging at 0.55 T and 1.5 T. *J Cardiovasc Magn Reson*. 2020;22(1):37. doi:10.1186/s12968-020-00618-y
17. Campbell-Washburn AE, Ramasawmy R, Restivo MC, et al. Opportunities in interventional and diagnostic imaging by using high-performance low-field-strength MRI. *Radiology*. 2019;293(2):384-393. doi:10.1148/radiol.2019190452
18. Gruetter R, Boesch C. Fast, noniterative shimming of spatially localized signals. in vivo analysis of the magnetic field along axes. *J Magn Reson*. 1992; 96:323-334.
19. Gruetter R. Automatic, localized in vivo adjustment of all first- and second-order shim coils. *Magn Reson Med*. 1993;29(6):804-811. doi:10.1002/mrm.1910290613
20. Bottomley PA. Spatial localization in NMR spectroscopy in vivo. *Ann N Y Acad Sci*. 1987;508(1):333-348. doi:10.1111/j.1749-6632.1987.tb32915.x
21. Haase A, Frahm J, Hänicke W, Matthaei D. ^{1}H NMR chemical shift selective (CHESS) imaging. *Phys Med Biol*. 1985;30(4):341-344. doi:10.1088/0031-9155/30/4/008
22. Bottomley PA, Foster TH, Argersinger RE, Pfeifer LM. A review of normal tissue hydrogen NMR relaxation times and relaxation mechanisms from 1–100 MHz: dependence on tissue type, NMR frequency, temperature, species, excision, and age. *Med Phys*. 1984;11(4):425-448. doi:10.1118/1.595535
23. Krššák M, Mlynárik V, Meyerspeer M, Moser E, Roden M. ^{1}H NMR relaxation times of skeletal muscle metabolites at 3 T. *Magn Reson Mater Phys Biol Med*. 2004;16(4):155-159. doi:10.1007/s10334-003-0029-1
24. Kreis R, Boer V, Choi IY, et al. Terminology and concepts for the characterization of in vivo MR spectroscopy methods and MR spectra: background and experts' consensus recommendations. *NMR Biomed*. 2020;34:e4347.
25. de Heer P, Bizino MB, Lamb HJ, Webb AG. Parameter optimization for reproducible cardiac ^{1}H-MR spectroscopy at 3 Tesla. *J Magn Reson Imaging*. 2016;44(5):1151-1158. doi:10.1002/jmri.25254
26. van der Meer RW, Doornbos J, Kozerke S, et al. Metabolic imaging of myocardial triglyceride content: reproducibility of ^{1}H MR spectroscopy with respiratory navigator gating in volunteers. *Radiology*. 2007;245(1):251-257. doi:10.1148/radiol.2451061904
27. Weiss K, Martini N, Boesiger P, Kozerke S. Cardiac proton spectroscopy using large coil arrays. *NMR Biomed*. 2013;26(3):276-284. doi:10.1002/nbm.2845
28. Gabr RE, Sathyanarayana S, Schär M, Weiss RG, Bottomley PA. On restoring motion-induced signal loss in single-voxel magnetic resonance spectra. *Magn Reson Med*. 2006;56(4):754-760. doi:10.1002/mrm.21015
29. Klose U. In vivo proton spectroscopy in presence of eddy currents. *Magn Reson Med*. 1990;14(1):26-30. doi:10.1002/mrm.1910140104
30. Vanhamme L, van den Boogaart A, Van Huffel S. Improved method for accurate and efficient quantification of MRS data with use of prior knowledge. *J Magn Reson*. 1997;129(1):35-43. doi:10.1006/jmre.1997.1244
31. Naressi A, Couturier C, Devos JM, et al. Java-based graphical user interface for the MRUI quantitation package. *Magn Reson Mater Phys Biol Med*. 2001;12(2/3):141-152. doi:10.1007/BF02668096

32. Boesch C, Slotboom J, Hoppeler H, Kreis R. In vivo determination of intra-myocellular lipids in human muscle by means of localized ^{1}H-MR-spectroscopy. *Magn Reson Med*. 1997;37(4):484-493. doi:10.1002/mrm.1910370403
33. Peereboom SM, Gastl M, Fuetterer M, Kozerke S. Navigator-free metabolite-cycled proton spectroscopy of the heart. *Magn Reson Med*. 2020;83(3): 795-805. doi:10.1002/mrm.27961
34. Boesch C, Machann J, Vermathen P, Schick F. Role of proton MR for the study of muscle lipid metabolism. *NMR Biomed*. 2006;19(7):968-988. doi:10.1002/nbm.1096
35. Ith M, Stettler C, Xu J, Boesch C, Kreis R. Cardiac lipid levels show diurnal changes and long-term variations in healthy human subjects. *NMR Biomed*. 2014;27(11):1285-1292. doi:10.1002/nbm.3186
36. Johnson JB. Thermal agitation of electricity in conductors. *Phys Rev*. 1928;32(1):97-109. doi:10.1103/PhysRev.32.97
37. Nyquist H. Thermal agitation of electric charge in conductors. *Phys Ther Rev*. 1929;32(1):110-113. doi:10.1103/PhysRev.32.110
38. Darrasse L, Ginefri JC. Perspectives with cryogenic RF probes in biomedical MRI. *Biochimie*. 2003;85(9):915-937. doi:10.1016/j.biochi.2003.09.016
39. Hasgall PA, Di Gennaro F, Baumgartner C, et al. IT'IS Database for Thermal and Electromagnetic Parameters of Biological Tissues. Version 4.0, May 15, 2018. doi:10.13099/VIP21000-04-0
40. Frass-Kriegl R, Hosseinnezhadian S, Poirier-Quinot M, Laistler E, Ginefri JC. Multi-loop radio frequency coil elements for magnetic resonance imaging: theory, simulation, and experimental investigation. *Front Physiol*. 2020;7:237. doi:10.3389/fphy.2019.00237

SUPPORTING INFORMATION

Additional supporting information can be found online in the Supporting Information section at the end of this article.

How to cite this article: Peereboom SM, Guenthner C, Albannay MM, Kozerke S. Preliminary experience of cardiac proton spectroscopy at 0.75 T. *NMR in Biomedicine*. 2023;36(7):e4892. doi:10.1002/nbm.4892

APPENDIX A

The time-domain SNR (SNR_{TD}) is defined as the maximum FID amplitude S divided by the standard deviation of the noise σ_{noise}:

$$\text{SNR}_{\text{TD}} = \frac{S(t=0)}{\sigma_{\text{noise}}}. \tag{A1}$$

The signal amplitude S is given by

$$S \propto \omega M_{xy}(\mathbf{x}) C(\mathbf{x}) \Delta V \tag{A2}$$

with ω denoting frequency, M_{xy} the transverse magnetization in volume element ΔV at position $\mathbf{x}$ and C the coil sensitivity. Given echo time $T_E \ll T_1$ and assuming 90° excitation and 180° refocusing pulses with perfect slice profiles, M_{xy} is given as

$$M_{xy}(\mathbf{x}) = M_0(\mathbf{x})\left(1 - e^{-\frac{T_R}{T_1(\mathbf{x})}}\right) e^{-\frac{T_E}{T_2(\mathbf{x})}} \tag{A3}$$

with $M_0 \propto B_0$ denoting the equilibrium magnetization and T_R the repetition time. Noise is described using the Johnson-Nyquist formula[36,37]:

$$\sigma_{\text{noise}} = \sqrt{4k_b (T_{\text{coil}} R_{\text{coil}} + T_{\text{sample}} R_{\text{sample}}) \text{BW}}, \tag{A4}$$

where k_b is the Boltzman constant, T_{coil} and T_{sample} denote the temperature of the coil and sample; R_{coil} and R_{sample} are the equivalent resistances of the coil and sample, respectively, and BW is the receiver bandwidth. In the frequency range considered, R_{sample} can be approximated according to Darrasse and Ginefri[38] as

$$R_{\text{sample}} = \frac{2}{3\pi} \sigma(\omega) \mu_0^2 \omega^2 r^3 \frac{\pi r}{8d} \tag{A5}$$

with $\sigma(\omega)$ the frequency- and hence field-dependent conductivity of the sample,[39] μ_0 the vacuum permeability, r the coil radius and d the distance between the sample and the coil. The intrinsic coil resistance R_{coil} for a single loop is calculated according to[40]

$$R_{\mathrm{coil}} = \frac{r}{q}\sqrt{\mu_0 \omega \frac{\rho}{2}}, \tag{A6}$$

where r is the coil radius, q is the radius of the coil wire and ρ is the electrical resistivity of the coil at temperature T_{coil} (copper resistivity taken from www.comsol.com). For the coil geometries used in this work and for field strengths above 0.5 T, $T_{\mathrm{sample}}R_{\mathrm{sample}}$ is greater than $T_{\mathrm{coil}}R_{\mathrm{coil}}$.

Besides the B_0 dependence of Equations (A2)–(A6), T_1 and T_2 are functions of B_0 as well and have been scaled with field strength according to[22]

$$T_1 = a(B_0)^b \tag{A7}$$

$$T_2 = c(B_0)^d \tag{A8}$$

with a, b, c and d being tissue-dependent constants, which are determined using ex vivo duck breast and in vivo calf muscle measurements in this work.

In relation to RF transmission, the time-averaged power P deposited in the subject is frequency dependent according to

$$P = \int_{\Delta V}\left(\sigma(\mathbf{x},\ \omega)\frac{1}{T_{\mathrm{R}}}\int_0^{T_{\mathrm{p}}}|E(\mathbf{x},\ \ t)|^2\,dt\right)d\mathbf{x}, \tag{A9}$$

where T_{p} denotes the duration of RF transmission. Since the electric field $E(\mathbf{x}, t)$ is proportional to the rate of change of the $B_1{}^{+}(\mathbf{x}, t)$ field generated by RF transmission of root-mean-square amplitude $B_{1,\mathrm{rms}}$ and pulse duration T_{p}, the frequency dependence of time-averaged power turns out to be

$$P \propto \sigma(\omega)\omega^2 \frac{B_{1,\mathrm{rms}}^2 T_{\mathrm{p}}}{T_{\mathrm{R}}}. \tag{A10}$$

For a given power limit P, it is seen that reducing ω allows for higher $B_1{}^{+}$. Approximating flip angle α by

$$\alpha \approx \gamma B_{1,\mathrm{rms}} T_{\mathrm{p}} \tag{A11}$$

and assuming $\sigma(\omega) \propto \omega^{0.25}$ for muscle tissue in the frequency range of 32–128 MHz[39] leads to

$$T_{\mathrm{p}} \propto \frac{\alpha^2 \omega^{2.25}}{P T_{\mathrm{R}}} \tag{A12}$$

which shows that T_{p} and therefore T_{E} can be decreased at lower field strength ($\omega \propto B_0$) by increasing $B_1{}^{+}$ while keeping the deposited time-averaged power P constant.

In the present work, and given power limits of coil components, linear scaling of RF pulse duration as a function of ω (and hence magnetic field) was implemented (see Equation 1). Accordingly, pulse durations were decreased linearly with decreasing field, provided peak $B_1{}^{+}$ was increased accordingly. It is noted that SAR depends on the average power deposited and hence scaling RF pulse amplitude and duration is an attractive opportunity at lower field.